Journal of Power Sources 487 (2021) 229416

Contents lists available at ScienceDirect

Journal of Power Sources

journal homepage: www.elsevier.com/locate/jpowsour

Phenyl TrifluoroMethane sulfonate as a novel electrolyte additive for enhancing performance of $LiNi_{0.6}Co_{0.2}Mn_{0.2}O_2$/Graphite cells working in wide temperature ranges

Jingxiong Gao [a,1], Songyi Han [b,1], Haiming Hua [a], Jie Wu [c], Jing Zeng [a], Yuanyu Sun [c], Weiping Tang [c,***], Shuling Liu [b,**], Jinbao Zhao [a,*]

[a] State Key Laboratory of Physical Chemistry of Solid Surfaces, Collaborative Innovation Centre of Chemistry for Energy Materials, State-Province Joint Engineering Laboratory of Power Source Technology for New Energy Vehicle, Engineering Research Center of Electrochemical Technology, Ministry of Education, College of Chemistry and Chemical Engineering, Xiamen University, Xiamen, 361005, PR China

[b] College of Chemistry and Chemical Engineering, Shaanxi Key Laboratory of Chemical Additives for Industry, Shaanxi University of Science & Technology, Xi'an, 710021, PR China

[c] State Key Laboratory of Space Power Technology, Shanghai Institute of Space Power-Sources (SISP), Shanghai Academy of Spaceflight Technology, Shanghai, 200245, PR China

HIGHLIGHTS

- A novel electrolyte additive used in the $LiNi_{0.6}Co_{0.2}Mn_{0.2}O_2$/graphite cell.
- Excellent electrochemical performance in wide temperature ranges.
- The thinner and more stable SEI films formed on the electrodes surface.
- The proposed possible reaction mechanism in the cell with PTM.

ARTICLE INFO

Keywords:
Phenyl trifluoromethane sulfonate
$LiNi_{0.6}Co_{0.2}Mn_{0.2}O_2$/graphite pouch cells
Wide temperature ranges
Electrolyte additive
Solid electrolyte interphase film

ABSTRACT

To optimize the electrochemical behavior of NCM-based high-energy lithium-ion batteries (LIBs) in wide temperature ranges, Phenyl trifluoromethane sulfonate (PTM) is demonstrated as the novel electrolyte additive to enhance the electrochemical behavior of $LiNi_{0.6}Co_{0.2}Mn_{0.2}O_2$/graphite cells at 25 °C, −20 °C and 45 °C. The cells with 1.0 wt% PTM-containing electrolyte deliver 80.6% capacity retention after 350 cycles at 25 °C, 73.4% after 100 cycles at −20 °C, and 82.6% after 300 cycles at 45 °C, which are significantly higher than that in standard electrolyte (STD), corresponding to 36.4% at 25 °C, 40.3% at −20 °C, and failure at 45 °C, respectively. According to density functional theory (DFT) simulations and quantitative calculations, the PTM preferentially reduces on the anode and oxidizes on the cathode to participate in the formation of solid electrolyte interphase (SEI) films. In addition, the scanning electron microscopy (SEM), Transmission electron microscope (TEM), X-ray photoelectron spectroscopy (XPS) and other analysis suggest that the formed SEI films are thinner and more stable for the electrolyte containing PTM, and the formed SEI films effectively control the decomposition of carbonate-based electrolytes and greatly decrease the increased resistance during the cycle.

1. Introduction

With the development of portable electronic devices, electric vehicles and other energy storage systems, the demand for LIBs is growing rapidly [1–3]. As a result of its high specific capacity, lithium nickel cobalt manganese oxides, $LiNi_xCo_y Mn_{1-x-y}O_2$ as the general

* Corresponding author.
** Corresponding author.
*** Corresponding author.
E-mail addresses: tangwp@sina.cn (W. Tang), shulingliu@aliyun.com (S. Liu), jbzhao@xmu.edu.cn (J. Zhao).
[1] These authors contributed equally.

https://doi.org/10.1016/j.jpowsour.2020.229416
Received 27 September 2020; Received in revised form 8 December 2020; Accepted 27 December 2020
Available online 5 January 2021
0378-7753/

formula, are the popular cathode materials used in LIBs [4,5], where the $LiNi_{0.6}Co_{0.2}Mn_{0.2}O_2$ (NCM622) has a better application prospect because of excellent cycle stability. However, due to its limited operating temperature range, the current commercial LIBs are far from meeting needs of various fields [6,7].

As we all know, the LIBs will accelerate aging while working at high temperature, and the performance of LIBs will decrease significantly, which is caused by the poor thermal stability of solvent molecules and lithium salt. The most important thing is that the electrolyte will be easier to produce a lot of gas while working under high temperature conditions, resulting in very fatal safety hazards [8,9]. Simultaneously, the LIBs will face the problem of huge capacity loss at low temperature, which is mainly due to the poor lithium transfer capacity of the formed SEI films on electrodes surface. The poor performance of the formed SEI film will lead to the significantly increased interface resistance and charge transfer resistance [10,11]. Even if LIBs work at room temperature, they will also experience varying degrees of capacity degradation during long-term cycle. In view of the above problems, optimizing the solvent system and adding film-forming additives are the main options to overcome these problems. Comparatively, adding film-forming additives has a lower cost and is more conducive to improving the diffusion of lithium ions on electrodes. In previous studies, many attempts have been made to solve the problems of LIBs at high or low temperature via the method of film-forming additives. Due to the strong reduction of fluoride, there have been many studies on fluorinated compounds as LIBs low temperature additives, including Fluoroethylene carbonate (FEC) [12], lithium tetrafluoroborate ($LiBF_4$) [13] and lithium bis(oxalato)borate (LiBOB) [14], which can optimize the components of SEI film to further optimize electrochemical behavior of LIBs working at low temperature. Due to the strong electronegativity of sulfur, the application of sulfur-containing organic additives to the high-temperature LIBs has also attracted people's interest. According to reports, 1,3-propanesultone (PS) [15], prop-1-ene-1,3-sultone (PES) [16], vinyl ethylene sulfite (VES) [17], 1,3,2-Dioxathiol ane-2,2-dioxide (DTD) [18], vinylene carbonate (VC) [19], as high-temperature additives, have also been discussed before. Recently, Among them, as the commercial electrolyte additive, 1,3-propanesultone (PS) can not only slow down the swelling process of the cells during the high-temperature cycles, but also enhance the performance of LIBs at room temperature and low temperature to a certain extent. However, the cells performance improved by PS is limited, which gradually unable to meet the development needs of LIBs. Even so, as far as we know, few additives are comparable to PS that can optimize the cells performance in wide temperature ranges. Therefore, we focus on improving the performance of LIBs in wide temperature ranges by selecting electrolyte additives containing aromatic rings, fluorine and sulfur, where the decomposition of additives containing aromatic ring may form aromatic ring products that are considered to be able to stabilize the SEI film due to their high stability.

In this paper, the PTM was firstly investigated as the electrolyte additive to enhance the electrochemical behavior of $LiNi_{0.6}Co_{0.2}Mn_{0.2}O_2$/graphite pouch cells in wide temperature ranges including low temperature and high temperature. For the cells with PTM-containing electrolyte, the cycle performance is improved obviously in wide temperature ranges. The electrochemical and physical characterizations have been employed to understand the influence mechanism on adding PTM to electrolyte, including SEM, TEM, and XPS, etc. Additionally, the DFT simulations and quantitative calculations have been applyed to infer the potential reaction mechanism of PTM in electrolyte.

2. Experimental section

2.1. Electrolytes and cells preparation

In this work, the STD was composed of which 1 M $LiPF_6$ dissolved in ethylene carbonate (EC), diethyl carbonate (DEC) ethyl methyl carbonate (EMC), with a 3:2:5 wt ratio. The above solvents and lithium salt were battery grade. The PS and PTM were both provided by Shanghai Aladdin Biochemical Technology Co., Ltd., which were added to the standard electrolyte in weight amounts of 1.0% to obtain the comparative electrolyte containing 1.0 wt% PS, the research electrolyte containing 1.0 wt% PTM, respectively.

The cathode slurry was prepared with a mixture of $LiNi_{0.6}Co_{0.2}Mn_{0.2}O_2$ (NCM622), conductive carbon (Super-P) and polyvinylidene fluoride (PVDF) with a 96.8:2.0:1.2 wt ratio, and evenly coated on the aluminum foil to obtain the cathode with 330 g m^{-2} areal density. The anode slurry was fabricated with a mixture of graphite, Carboxymethyl Cellulose (CMC), Super-P and Polymerized Styrene Butadiene Rubber (SBR) with a 95:1.5:1.5:2 wt ratio, and uniformly coated on the copper foil to obtain the anode with 185 g m^{-2} areal density. In addition, the Polyethylene film was selected as separator. The pouch cells were assembled by the above-mentioned electrodes and 6g electrolyte was injected into each cell.

2.2. Electrochemical tests and characterization analysis

The electrochemical window of the electrolyte with or without PTM was tested by linear sweep voltammetry (LSV) at a scanning speed of 1 mV/s and the voltage range was 3.0 V–6.5 V (V vs. Li/Li^+), where the lithium metal was regarded as reference and counter electrodes and the platinum as working electrode. The charge-discharge cycle performance tests of pouch cells with PS or PTM were conducted with 1 C rate in voltage range of 2.75–4.2V at different temperatures including 25 °C,-20 °C and 45 °C (Neware, CT-3008W–5V/6A, China). The cycle stability and coulombic efficiency of half cells with or without PTM were conducted with 1 C rate at 25 °C. At the same time, the pouch cells containing STD electrolyte were tested under the same conditions, which were regarded as the reference experiments. It is worth noting that, before the charge-discharge cycle performance tests at different temperatures, all cells were kept in an electro-thermostatic oven (Shanghai CIMO Medical Instrument Manufacturing Co., Ltd.,) with the test temperature for 4 h. The high temperature storage performance of the cells with or without PTM were evaluated at 60 °C for 10 days. Specially, all tested cells were charged and discharged at 1 C rate for three cycles, then they were fully charged again and transferred to the thermostat oven. Before and after elevated temperature storage, the electrochemical impedance spectroscopy (EIS) of cells was measured by the frequency response analyzer (FRA, Solartron 1455A, UK) from 10 mHz to 100 kHz and the amplitude disturbance was 10 mV. In order to analyze the difference on the performance of cells with and without PTM in the charge-discharge cycle performance tests, taking the cycle at 25 °C as an example, the EIS tests were carried out on the cells after 350 cycle.

To further figure out the changes of the electrodes surface before and after the cycle in different electrolytes, taking the cycle at 25 °C as an example, the electrodes collected from the cycled cells were washed by DMC. Then, the treated electrodes were transferred into the argon-filled glove until dried. The morphology characterizations of different electrodes surface were observed by SEM (ZEISS Ultra 55). The thickness and uniformity of SEI films were observed by TEM (JEOL 2100F), The crystal structure changes of cycled cathodes were characterized by X-ray diffraction (XRD, Rigaku D/Max2500). The chemical compositions on different electrodes surface were determined by X-ray photoelectron spectroscopy XPS (Axis Ultra DLD). The Inductive Coupled Plasma (ICP) test was used to measure the specific content of transition metal ions in the cycled anode by ICP-AES 7510.

2.3. Computational details

All DFT calculations were performed by using Gaussian09 E01 [20] software. The geometries of molecules were optimized with B3LYP-D3 [21,22] density functional and def2-SVP [23] basis set. The continuum solvation model SMD [24] was used to calculate solvent effect in

EC/DEC/EMC electrolyte. The relative dielectric constant(ε) of the electrolyte was 28.9 and parameters of non-polar parts were same as ethyl ethanoate. Frequency analysis was performed to ensure that all the structures were the minimum points on potential energy surface. Mayer bond order was calculated by using Multiwfn [25] software to measure the bond strength.

3. Results and discussion

3.1. Characteristics of PTM and electrolytes containing PTM

By comparing the orbital energy of molecules and combining quantitative calculations, the potential reaction of electrolyte during the cycle can be predicted. Based on the frontier orbital theory, the molecule with higher HOMO orbital energy is more likely to be oxidized, and the molecule with lower LUMO orbital energy is more easily to be reduced [26]. According to the results shown in Fig. 1a, the PTM possesses a higher HOMO (−7.3097 eV) orbital energy and a lower LUMO (−3.9123 eV) orbital energy than that of EC (−8.226 eV, 0.1818 eV), EMC (−7.7531 eV, 0.5614 eV) and DEC (−7.6774 eV, 0.6299 eV), which can be inferred that the PTM is prior to participate in reduction reaction on anode and oxidation reaction on cathode compared to other components, and has a hand in the formation of the interface film. In addition, the PS molecule possesses a higher LUMO (−2.3607 eV) orbital energy and a lower HOMO (−7.8302 eV) orbital energy compared to PTM shown in Fig. S6, suggesting that PTM is more oxidizing and reducing.

In order to have a clearer understanding of PTM and prepare for the subsequent speculation of the reaction mechanism, quantitative calculations were used to understand the changes in the bond length (Å) of PTM while obtaining or losing an electron. As shown in Fig. 1b, while getting an electron on the anode, the O12–S13 bond length was significantly increased from 1.41 Å to 2.55 Å and the C3–O12 bond length was decreased from 1.64 Å to 1.29 Å, which indicated the O12–S13 was about to break. While losing an electron on the anode, the O12–S13 and the C3–O12 bonds length were changed to 1.85 Å and 1.33 Å, respectively, which was the same as the change trend after obtaining an electron and meant the O12–S13 was also likely to break. The result suggested that PTM may modify the composition of the SEI film to affect cells performance by breaking O12–S13.

The LSV was employed to compare the electrochemical stability of electrolytes before and after adding PTM shown in Fig. S1. For the STD electrolyte, the oxidation current increased rapidly when the potential approached 5.7V, which indicated that the electrolyte would be subjected to the severe oxidative decomposition once the potential exceeded 5.7V. While the decomposition potential of the electrolyte containing PTM was broadened to 6.2V. However, what we need to pay attention to is that a significant oxidation current appeared at about 4.55V in the electrolyte containing PTM, which was due to the preferential oxidation of PTM. In addition, the electrolyte containing PS delivered a lower decomposition potential of 6V compared to the one containing PTM. According to these result, we believed that PTM as the electrolyte additive better enhanced the electrochemical stability of the electrolyte by its preferential oxidation.

3.2. Electrochemical properties of pouch cells with PTM

It is worth noting that, in order to better illustrate that PTM as the

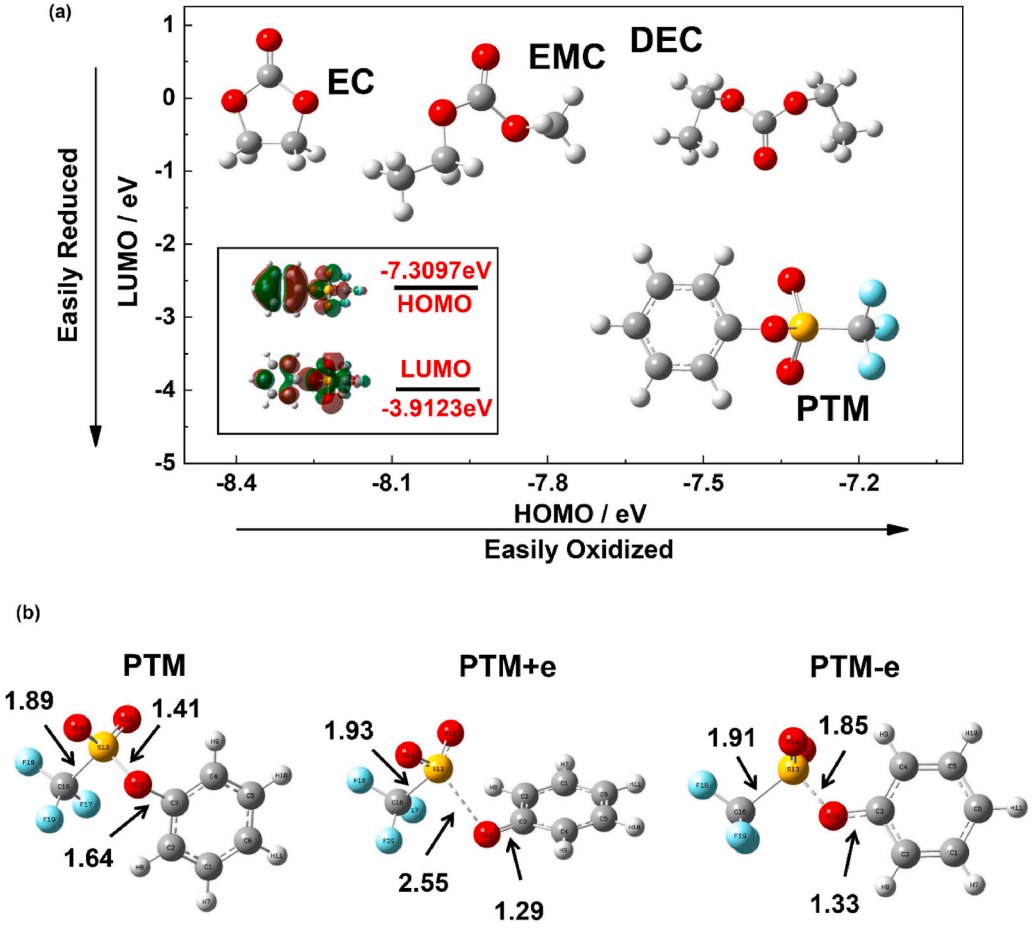

Fig. 1. (a) The calculated HOMO/LUMO values of EC, DEC, EMC and PTM molecules; (b) C3–O12, O12–S13 and S13–C16 bond lengths (Å) of PTM molecule before and after getting or losing an electron.

electrolyte additive can significantly enhance the performance of the cells, we chose the currently commercialized PS additive as the comparative test. The cycle performances of the cells with or without PTM at different temperatures were compared shown in Fig. 2. Fig. 2a and b showed the cycle performance and coulombic efficiency of $LiNi_{0.6}Co_{0.2}Mn_{0.2}O_2$/graphite pouch cells cycled in the STD electrolyte at 25 °C, PS-containing electrolyte at 25 °C and PTM-containing electrolyte at 25 °C, respectively. It can be clearly seen that the pouch cells cycled in the STD electrolyte exhibited a rapid capacity decay, which delivered the low capacity retention of 36.4% after 300 cycles. The same situation corresponded to the electrolyte containing PS. Although the cycle performance of the cells with PS-containing electrolyte was slightly improved, its capacity retention rate was only 57.3%. In contrast, the cells with PTM-containing electrolyte achieved excellent cycle performance, which possesed the high capacity retention of 80.6% after 350 cycles. In addition, it is not difficult to see that the cells with PTM-containing electrolyte remained more stable coulombic efficiency during the cycle. Since then, we believed that the cycle stability of cells at 25 °C was significantly improved by choosing PTM as the electrolyte additive.

As shown in Fig. 2c and d, the influence of PTM on cycle performance of the pouch cells was explored at −20 °C. As we all know, the slow lithium kinetics on graphite is the main reason for the rapid decline of cells capacity at low temperature [27]. Therefore, the initial capacity of cells with different electrolytes all showed varying degrees of attenuation compared to 1805.78 mAh at 25 °C, corresponding to 1262.12 mAh for STD, 1142.84 mAh for PS and 1458.28 mAh for PTM, respectively. Additionally, the cells with STD or PS experienced a fast capacity fading to 509.77 mAh and 882.23 mAh after 100 cycles at −20 °C, which was also consistent with the instability of coulombic efficiency in Fig. 2d. However, a clear contrast was showed in Fig. 2c when the cells cycled in PTM-containing electrolyte. The cells with PTM still maintained

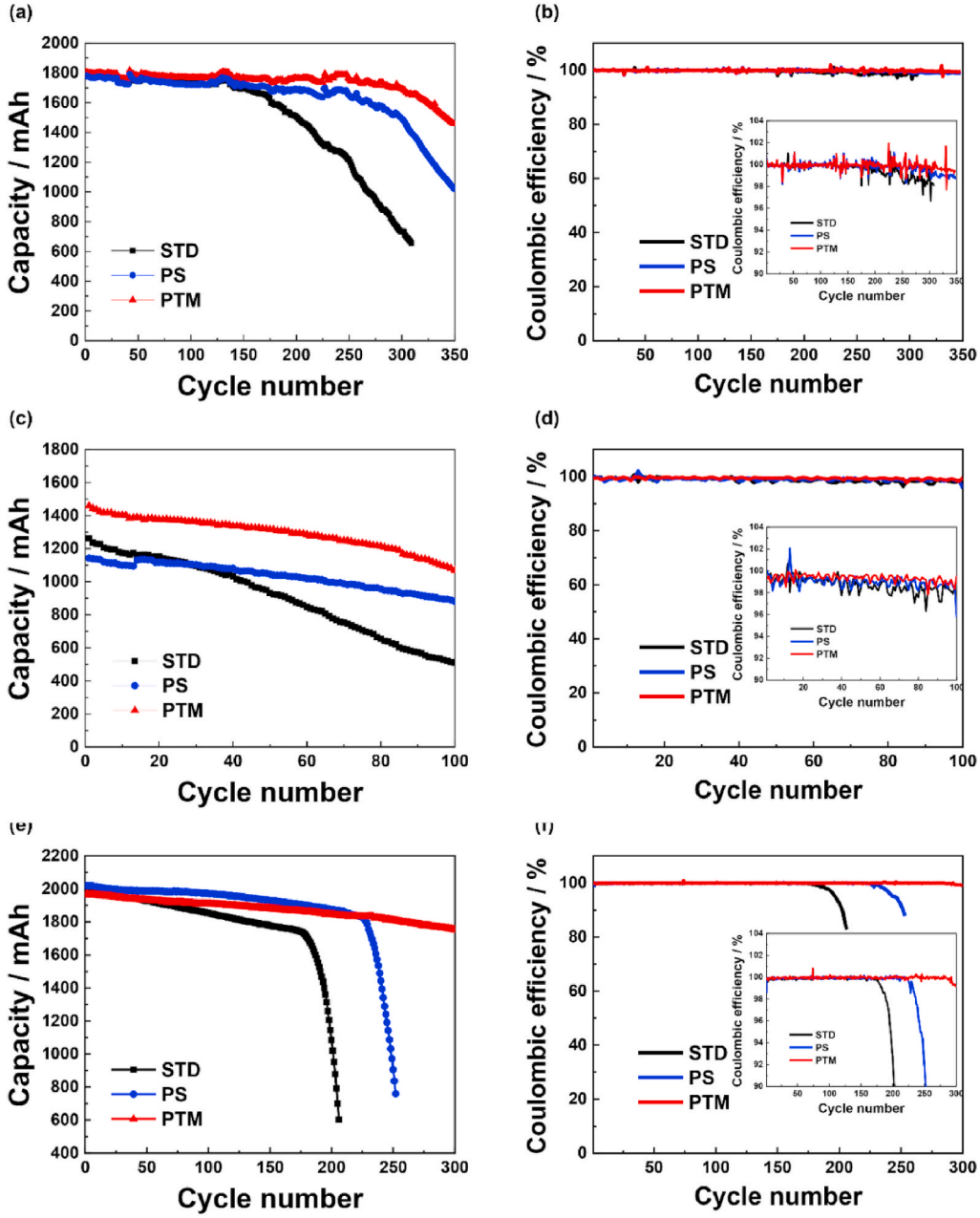

Fig. 2. Cycle performance and coulombic efficiency of $LiNi_{0.6}Co_{0.2}Mn_{0.2}O_2$/graphite full cells with 1 C in a voltage range of 2.75–4.20V at various temperature: (a), (b) 25 °C; (c), (d)-20 °C; (c), (d) 45 °C.

1070.39 mAh after 100 cycles, which was significantly better than the cells without PTM. The above results suggested that the addition of PTM obviously optimized the cycle performance of cells cycled at low temperature.

In order to understand whether PTM as the electrolyte additive can enhance cells performance at high temperature, we also investigated the cells containing PTM cycled at 45 °C. As depicted in Fig. 2e, although the cells with different electrolyte systems all exhibited the nearly same initial discharge capacity (2000.00 mAh), there were completely different performances in subsequent cycles. For the cells containing STD, they delivered extremely poor cycle stability. Especially, the cells capacity dropped sharply after 200 cycles, corresponding to the significantly decreased coulombic efficiency in Fig. 2f, which may be due to the massive loss of reversible lithium and the destruction of the electrode surface structure by the decomposition products from carbonate-based electrolyte and $LiPF_6$ during the cycle. The cells containing PS delivered relatively good cycle performance until 250 cycles. Surprisingly, the cells containing PTM exhibited extremely superior cycle stability, which achieved a little capacity fade and maintained 1651.69 mAh (82.6%) after 300 cycles. The coulombic efficiency of cells with PTM also showed the same excellent results in Fig. 2f. Apparently, the cycle performance of cells cycled at high temperature was greatly improved by adding PTM to electrolyte.

There are three possible explanations for the enhanced cycle performance of the cells with PTM at different temperatures. On the one hand, the protective and uniform SEI film was formed on the electrodes surface during the cycle, which can prevent the destruction of electrodes by carbonate-based electrolytes and their decomposition products. Another is that the cells with PTM have the lower interface resistance and charge transfer resistance, which can promote the conduction of lithium on the electrodes surface. The last one is that PTM preferentially reduced on anode and oxidized on cathode in the electrolyte system and suppressed the decomposition of other components, which can be judged from the LUMO and HOMO value in the calculation part. The following methods were employed to support these views.

Fig. S4a and b displayed the cycle stability and coulombic efficiency of half cells cycled in the electrolyte with or without PTM additive, respectively. The graphite electrode was charged/discharged at 0.005–2.5 V with 0.1 C for first three cycles and 1 C for remaining cycles at 25 °C shown in Fig. S4a. And the $LiNi_{0.6}Co_{0.2}Mn_{0.2}O_2$ electrode was charged/discharged at 2.75–4.2 V with 0.1 C for first three cycles and 1 C for remaining cycles at 25 °C shown in Fig. S4b. A significant capacity fading was observed for electrodes cycled in the electrolyte without PTM for 120 cycles, with the low coulombic efficiency (99.2%) and remaining capacity of 263.1 mAh g^{-1} for graphite electrode, the low coulombic efficiency (96.3%) and capacity retention of 55.5% for $LiNi_{0.6}Co_{0.2}Mn_{0.2}O_2$ electrode. The poor cycle performance was attributed the poor stability of electrolyte and damaged electrodes by decomposition products of electrolyte. In contrast, when PTM was applied in electrolyte, an excellent performance was delivered after 120 cycles (the higher coulombic efficiency of 99.8% and remaining capacity of 337.3 mAh g^{-1} for graphite electrode; the higher coulombic efficiency of 97.9% and capacity retention of 82.1% for $LiNi_{0.6}Co_{0.2}Mn_{0.2}O_2$ electrode), suggesting that PTM can not only improve the stability of electrolyte and effectively protect the electrodes from the destruction of electrolyte decomposition products.

3.3. Impedance analysis

To further explore the contribution of PTM to the high temperature performance of $LiNi_{0.6}Co_{0.2}Mn_{0.2}O_2$/graphite cells, the high temperature storage experiment test was conducted by EIS shown in Fig. 3a and b. For convenience, we considered the semicircle as only the charge transfer resistance (R_{ct}) for analysis. It is noteworthy that the impedance

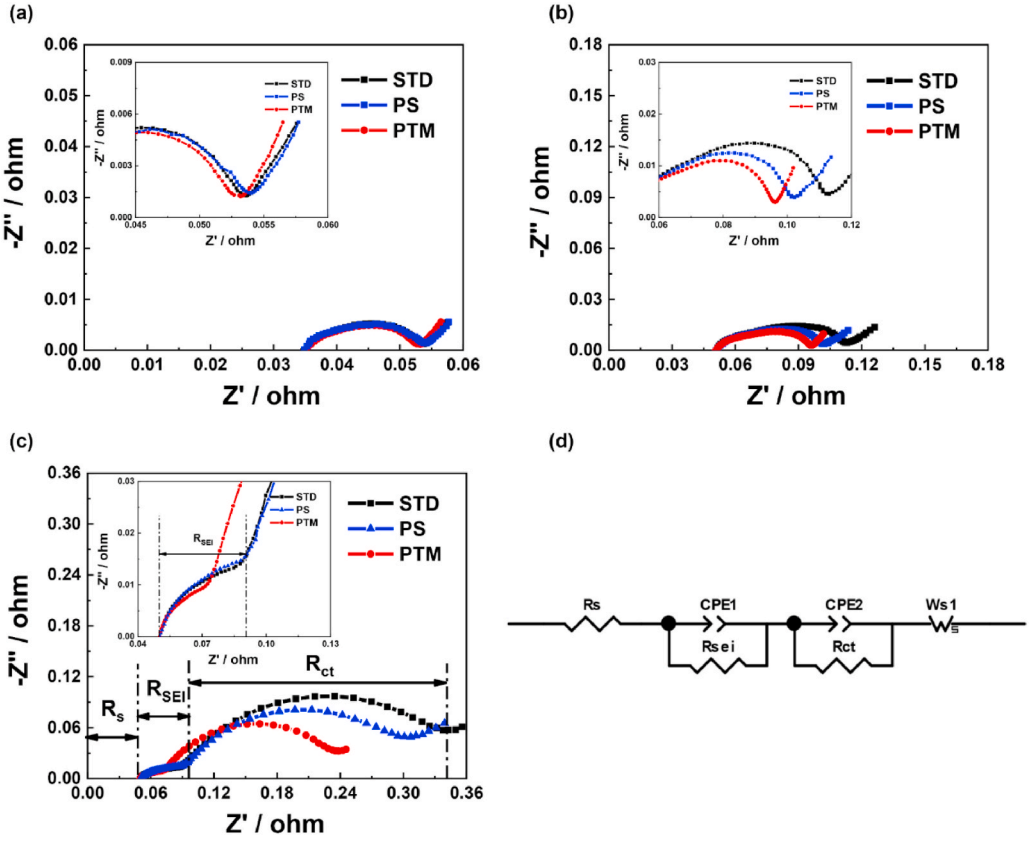

Fig. 3. EIS of $LiNi_{0.6}Co_{0.2}Mn_{0.2}O_2$/graphite full cells with STD electrolyte and the electrolyte with PS or PTM: (a) initial impedance; (b) after storage; (c) after over 300 cycles at 25 °C; (d) relevant equivalent circuit.

spectra of different electrolytes systems showed different growth trends after storage at 60 °C for 10 days, even all delivered approximately the same initial impedance in Fig. 3a. The above result indicated the impedance of the cells containing STD increased significantly after high temperature storage, which was attributed to the poor thermal stability of the formed SEI film. Additionally, the SEI film with poor performance did not withstand the attack of the harmful products produced by the decomposition of $LiPF_6$ on electrodes and the accumulation of by-products hindered the diffusion of lithium [28], leading to an increase in cells impedance. Obviously, PS as the electrolyte additive effectively suppressed the increase of cells impedance during high temperature storage. But the impedance of cells containing PTM was better suppressed than that with PS, which was attributed to the SEI film with great thermal stability derived from PTM that alleviated the accumulation of by-products produced by carbonate-based electrolyte and $LiPF_6$ decomposition to promote the diffusion of lithium.

To determine the differences in the interface impedance of cells cycled in different electrolytes, taking the cycle at 25 °C as an example, the impedance of pouch cells after cycling was measured by EIS depicted in Fig. 3c. The EIS curve was divided into four parts: Super high frequency as total resistance of cell (R_s), high frequency semicircle as interfacial resistance (R_{SEI}), low frequency semicircle as charge R_{ct} and low frequency line as Warburg resistance, respectively, and fitted an equivalent circuit shown in Fig. 3d. Apparently, from the quivalent circuit datas in Table S1, the increased R_{SEI} was significantly suppressed by adding PTM, which was attributed to the formed SEI film with excellent conductivity and stability on the electrodes surface. And we all know that a lower R_{SEI} was more beneficial for lithium to transmit

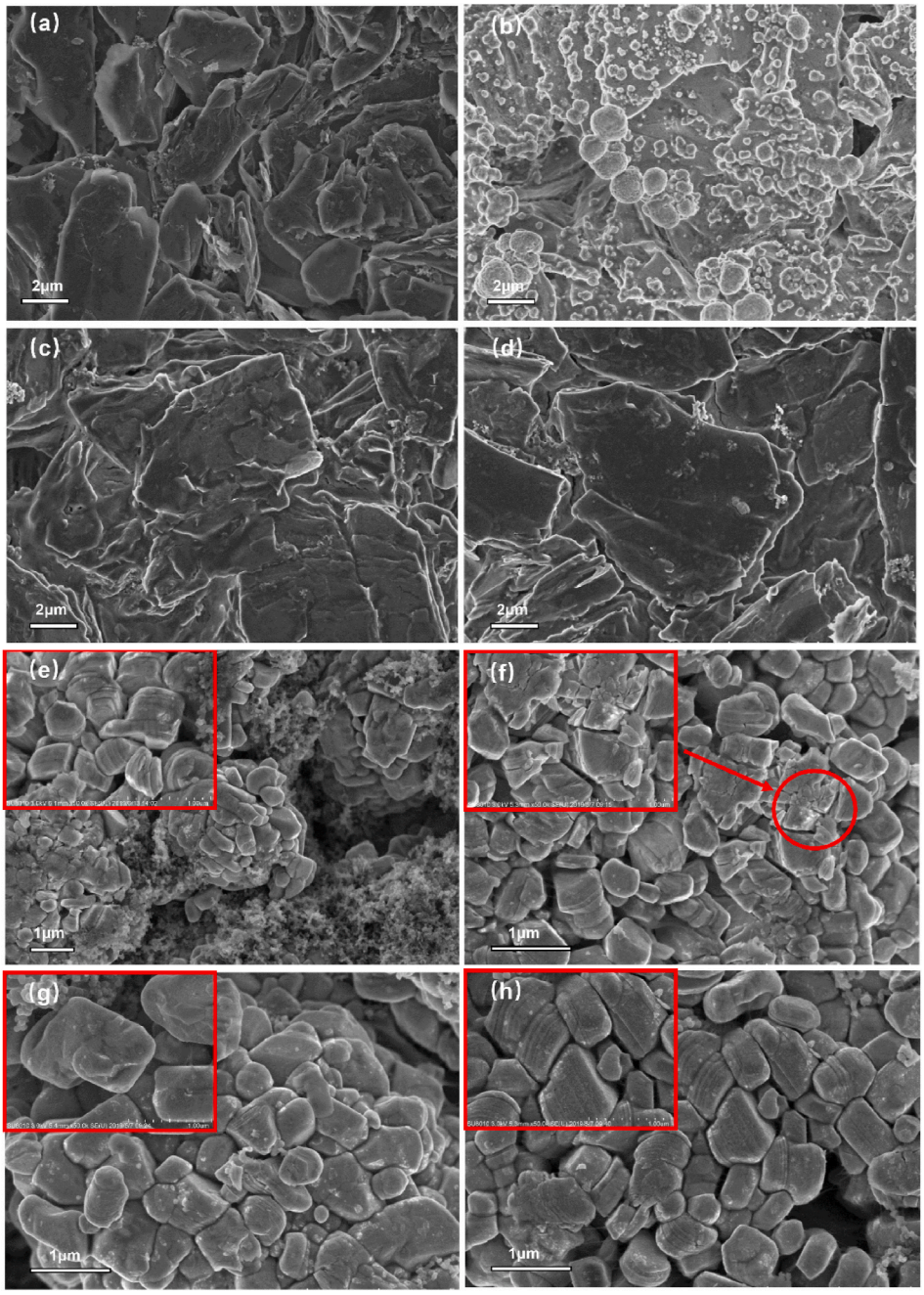

Fig. 4. SEM images of the electrodes: (a) fresh graphite anode; (b) cycled anode with STD; (c) cycled anode with PS; (d) cycled anode with PTM; (e) fresh NCM622 cathode; (f) cycled cathode with STD; (g) cycled cathode with PS; (h) cycled cathode with PTM.

between electrodes and electrolyte. Meanwhile, a sharply lower R_{ct} in cells with PTM was easily found, corresponding to the reduction of non-conductive decomposition substances produced by carbonate-based electrolytes deposited on electrodes surface. Consequently, the pouch cells with the PTM-containing electrolyte can form the better performance SEI film during the cycle, which not only promoted migration of lithium between electrodes and electrolyte, but also reduced the decomposition of carbonate-based electrolytes.

3.4. Structure and morphology analysis of electrodes

The surface morphology of the fresh electrodes and the cycled electrodes with different electrolytes after over 300 cycles at 25 °C was presented by SEM characterization. Obviously, there were clear differences on the cycled electrodes surface in Fig. 4. Compared to the changes in the morphology of cathode surface, more distinctive differences existed on the morphology of graphite surface. The morphology of graphite cycled in the STD electrolyte changed significantly was shown in Fig. 4b, which was covered by a large number of by-products produced by electrolytes compared to the fresh one. When the PS additive was added to the electrolyte, there were not excessive by-products but obvious protruding flaky shape structure on graphite surface in Fig. 4c, which implied that the graphite suffered from the destruction of electrolyte during the prolong cycle. On the contrary, a thin and uniform layer was covered on the cycled graphite surface with the PTM-containing electrolyte, and the smooth and unobstructed graphite surface was displayed in Fig. 4d. With regard to the reasons for the above results, it may be mainly due to the following reasons: due to its strong reducibility, the PTM was prior to decompose on the graphite surface than that for EC, EMC and DEC, which alleviated the decomposition of carbonate-based electrolytes. In addition, the PTM greatly ameliorated the property of the SEI film, which can effectively protected the integrity of the graphite structure.

NCM622 particles with complete structure were distributed on the surface of the fresh cathode and a few small particles representing PVDF and Super-P adhered to the NCM622 particles shown in Fig. 4e. However, for the cathode cycled in the STD electrolyte for 300 cycles (Fig. 4f), some uneven particles occurred on the cycled cathode surface, which contributed to the high interface resistance and poor cycle performance. Simultaneously, from the inset in Fig. 4f, it is easy to find that the structure of NCM622 particles was destroyed during the cycle. The above-mentioned inferior surface morphology may be due to the lack of the SEI film with effective protection. Therefore, the cathode suffered from electrolyte erosion and was affected by the decomposition products of the carbonate-based electrolyte. Differently, morphology integrity of the NCM622 particles cycled in PS-containing electrolyte was relatively well-preserved shown in Fig. 4g, but still with a small amount of by-product particles. Surprisingly, in Fig. 4h, the cycled cathode acquired from the cells with PTM did not encounter the above problems, and the visible layered structure of NCM622 particles was depicted in the inset of Fig. 4h. In conjunction with the performance of different cells during the cycle, we believed that the thin and uniform SEI film was formed on the cathode surface when PTM was present, and which prevented the direct contact between electrolyte and cathode to realize the protection of NCM622 particles. Moreover, the oxidative decomposition of solvent molecules was suppressed due to the strong oxidizing of PTM.

In order to further illustrate the changes in crystal structure of NCM622 cathode before and after the cycle with or without PTM at 25 °C, as shown in Fig. S2, the XRD measurements were employed to deliver differences. For NCM622 cathode cycled in the STD electrolyte, the diffraction peak intensity was significantly decreased. Especially, the peaks of (015), (107) and (113) nearly disappeared, indicating that the structure of NCM622 cathode was severely damaged during the cycle. In contrast, there were almost no changes between the pristine cathode and the cycled cathode with PTM-containing electrolyte, suggesting the structure of the NCM622 cathode with PTM-containing electrolyte was well-preserved. In detail, the peaks of (018)/(110) and (006)/(102) can be clearly observed in the system containing PTM shown in Fig. S2b, corresponding to the complete layered structure of NCM622 particles [29]. The XRD test results of the cycled cathode were completely consistent with the SEM analysis. Thus, while cycling in the PTM-containing electrolyte, we believed that the stable and uniform SEI film ensured the integrity of the cathode structure.

TEM analysis was conducted to compare the thickness and uniformity of the SEI film for the electrodes with and without PTM. Fig. S3 displays the TEM images of the anode and cathode with and without PTM after over 300 cycles at 25 °C. As shown, there was obviously different on the morphology of the SEI films on the graphite surface. Partially clear graphite contour edges were observed on the cycled anode surface without PTM in Fig. S3a, indicated the SEI layer did not completely cover the graphite surface. Differently, the denser and thinner SEI was observed on the graphite surface with PTM, and the graphite surface was completely covered, which was beneficial to reduce the influence of transition metal ions on graphite anode. Similarly, the SEI film formed on the cycled cathode surface without PTM was also incomplete shown in Fig. S3c. In contrast, the cathode surface with PTM was completely covered by uniform and thin SEI layer in Fig. S3d. The above TEM results indicated that the formed SEI films on the electrodes surface with PTM were more uniform and thinner, which effectively prevented electrodes corrosion from electrolyte and decreased the interface resistance.

3.5. XPS analysis of cycled electrodes

To further support the views that PTM did participate in the formation of SEI film and optimized the composition of SEI film during the cycle, the surface chemical elements of both anode and cathode cycled in the electrolyte containing PTM or not at 25 °C were compared by XPS analysis. First of all, in the C 1s spectrum of cycled graphite shown in Fig. 5, the graphite with PTM displayed the lower content of C═O (288.5 eV) and nearly disappeared Li_2CO_3 (289.9 eV) compared to the graphite with STD, corresponding to the reduced decomposition of carbonate-based electrolytes. Thus, when the PTM was added in electrolyte, the reductive decomposition of carbonate-based electrolyte on the anode surface was well suppressed, which was consistent with the SEM results. The C–C peak (284.6 eV) intensity of graphite with PTM was obviously higher than the one of graphite without PTM, which was due to the formation of the thinner SEI film on graphite surface while cycling in PTM-containing electrolyte and the additional C–C bonds contributed by the PTM (C–C═C). Whether or not PTM was added to the electrolyte, both C–O peaks (286.4 eV) intensity belonged to CMC binder was very low. However, it is not difficult to find that the C–O peak (286.4 eV) intensity of graphite with PTM was slightly higher than that of graphite with STD, which again indicated the thickness of SEI film formed on the surface of graphite cycled in the PTM-containing electrolyte was thinner than that of graphite cycled in the STD electrolyte, corresponding to the TEM test results.

For the O 1s spectra of cycled graphite, the peaks near 533.1 eV, 532.1 eV and 531.4 eV corresponded to C–O, C═O and Li_2CO_3, respectively. The content of C═O and Li_2CO_3 also decreased when the PTM was added to the electrolyte. The information obtained from the O 1s spectrum was consistent with that obtained from the C 1s spectrum, which both indicated the reductive decomposition of carbonate-based electrolyte was inhibited by adding PTM.

In the F 1s spectrum, the characteristic peak of LiF appeared at 684.8 eV, which was due to the decomposition of $LiPF_6$. However, it is worth noting that, with the decomposition of $LiPF_6$, HF and PF_5 that were considered as the key role in destroying the electrode-electrolyte interface also appeared [30]. The peak intensity of LiF with PTM was significantly distinct with that of LiF without PTM, and the former peak basically disappeared. The result directly explained that when the PTM as additive was added into the electrolyte, the decomposition of $LiPF_6$

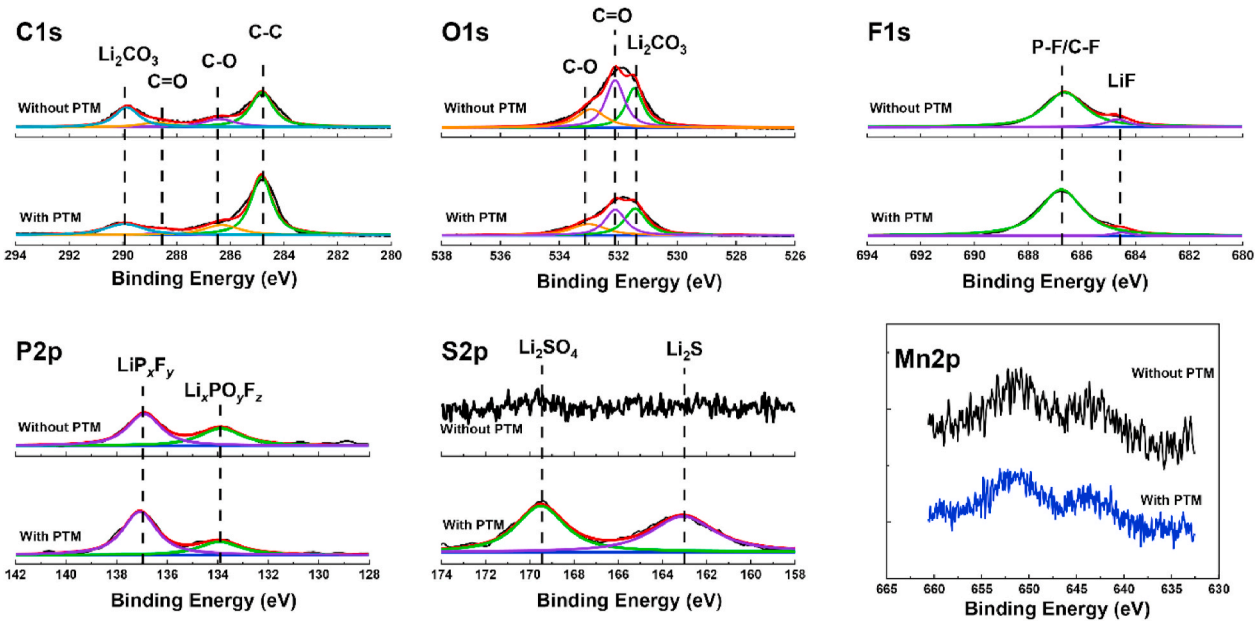

Fig. 5. The XPS spectras of the graphite anodes with and without PTM after over 300 cycles at 25 °C.

was well controlled. The peak at 686.8 eV corresponded to P–F, belonged to Li_xPO_yF and LiP_xF_y. Among them, the Li_xPO_yF was considered to be the decomposition product of $LiPF_6$, and the LiP_xF_y was regarded as the undecomposed $LiPF_6$. In conjunction with the P2p spectrum, both the higher content LiP_xF_y (137 eV) and the lower content Li_xPO_yF (133.9 eV) in the graphite with PTM again illustrated that the decomposition of $LiPF_6$ rarely occurred when the graphite anode cycled in the electrolyte containing PTM. Additionally, the C–F at 686.8 eV originated from the Hexafluoroethane that was a decomposition product of PTM.

For the S2p and Mn2p spectra, the new peaks appeared at 169.4 eV (Li_2SO_4), 163 eV (Li_2S) in the S2p spectra of graphite with PTM, where parts of Li_2S and Li_2SO_4 were the further disproportionation reaction products of Li_2SO_3, which was all attributed to the broken O12–S13 bond from PTM when the PTM got an electron. Related studies [31,32] have suggested that the above-mentioned salts adhering to the electrode surface can promote the lithium diffusion between electrodes and electrolyte. Besides, in the Mn2p spectra, the lower Mn element content was easily found on the PTM-containing graphite surface. Compared to the electrolyte without PTM, the lower Ni and Co elements content was also easily found on the PTM-containing graphite surface shown in Figs. S9a and b. The same results as Mn element all indicated that the formed SEI film by PTM can block the transfer of transition metal ions to anode. In addition, the specific content of transition metal ions in the cycled anode was measured by ICP test and the results were shown in Table S2. According to these results, we can conclude that the PTM did participate in the formation of SEI film on the graphite surface and the formed SEI film was more stable and more conducive to the lithium conduction on the SEI film.

The composition changes on the cathode surface were depicted in

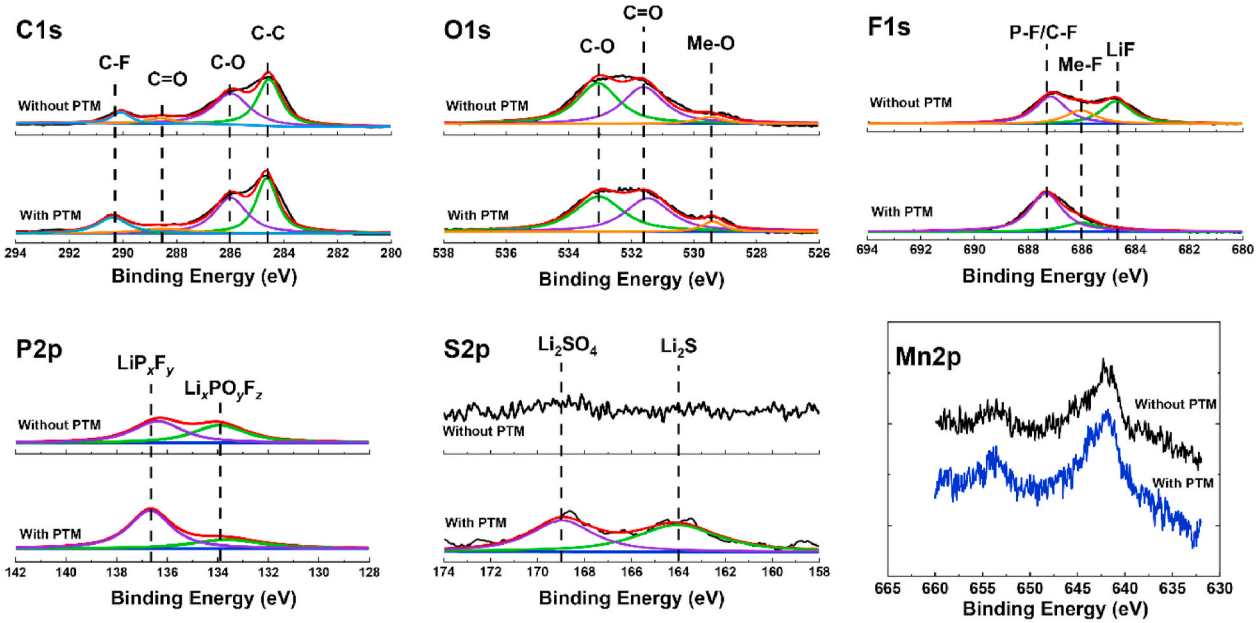

Fig. 6. The XPS spectras of the NCM622 cathodes with and without PTM after over 300 cycles at 25 °C.

Fig. 6. For the C 1s spectra, the peaks appearing at 284.6 eV was regarded to the C–C of conductive carbon (Super-P) and that of PTM (C–C═C), and the peak of C–F was observed at 290.4 eV belonged to the PVDF binder. Compared with the cathode cycled in STD electrolyte, the above peaks were clearer for the cathode cycled in PTM-containing electrolyte, which indicated that the thinner SEI film was formed on the cathode surface with PTM, corresponding to TEM analysis. And the thinner SEI film corresponded to the lower interface impedance. The peaks around 286 eV and 288.6 eV assigned to the C–O and C═O of Lithium carbonate, which was a major oxidation decomposition product of carbonate-based electrolyte. Thus, we were aware that, when the PTM was added into electrolyte, the SEI film formed on the cathode surface inhibited the oxidative decomposition of carbonate-based electrolyte. Similarly, the results obtained from the O 1s spectra were same as those obtained from C 1s spectra. In addition, the Me–O was mainly derived from the fresh cathode, and less content meant the thinner SEI film [33]. The results observed from F 1s spectrum, P 2p spectrum and S 2p spectrum were almost the same as those on the anode, which showed

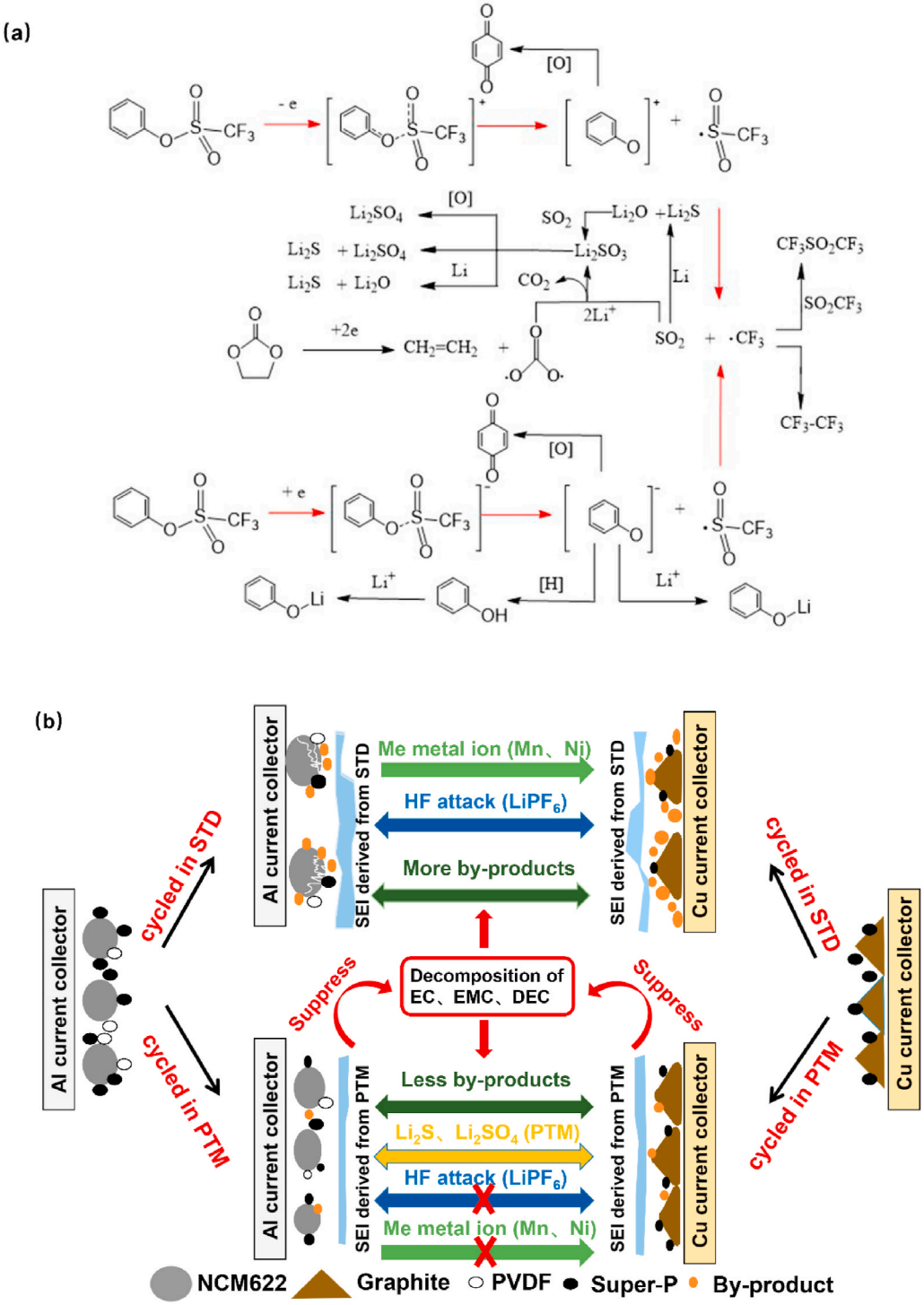

Fig. 7. (a) Possible reaction mechanism of the PTM molecule participating in the formed SEI films on electrodes surface; (b) schematic diagram of the formed different SEI films on the electrodes of the $LiNi_{0.6}Co_{0.2}Mn_{0.2}O_2$/graphite with and without PTM during the cycle.

that the PTM as the electrolyte additive took part in the formation of SEI film on cathode surface and improved the conductivity and stability of SEI film. Furthermore, a slight difference appeared in the Mn2p spectra, where the Mn element was attributed to the NCM622 material, and the Mn content in the cathode with PTM was higher as a result of the thinner SEI film.

In addition, the XPS spectras of the graphite anode and NCM622 cathode with PS were shown in Fig. S7 and Fig. S8, respectively. Whether it is anode or cathode, the high content of C–C (284.6 eV) and C–O (286.4 eV) in the C 1s spectra indicated that the formed SEI films on the electrodes surface with PS were thin, and the peak at 533.1 eV in the O 1s spectra also illustrated it. However, the peaks at 532.1 eV (C═O) and 531.4 eV (Li_2CO_3) in the O 1s spectra of graphite anode were obviously higher than those with PTM, suggesting more decomposition of carbonate-based electrolytes occurred in the system containing PS compared to the one containing PTM. In addition, a higher peak at 684.8 eV (LiF) in the F 1s spectra and a lower peak at 137 eV (LiP_xF_y) in the P 2p spectra corresponded to more decomposition of $LiPF_6$. And more transition metal ions were detected on the anode with PS in Figs. S9c and d, indicating the formed SEI films did not effectively block the transfer of transition metal ions to anode. Therefore, the formed SEI films on the electrodes surface with PS were thin but unstable.

As shown in Fig. 7a, the possible reaction mechanism in the containing PTM electrolyte system was proposed, corresponding to the XPS analysis to better comprehend the role of PTM in the electrolyte system. For the reaction on the anode surface, once obtaining an electron, PTM will preferentially reduce by breaking the O12–S13 bond to form sulfur-based lithium salt on the anode surface which were conducive to the conduction of lithium at the interface. In addition, a small amount of aromatic ring compounds will also adhere to the anode surface, which is considered to improve the stability of SEI film as a result of their aromatic ring structure [34]. And the fluorine element in PTM makes the O12–S13 bond easier to break due to its high polarity, and finally forms the hexafluoroethane. For the reaction on the surface of the cathode, the PTM will also break the O12–S13 bond while losing an electron. Therefore, the decomposition products derived from PTM on the cathode surface are basically consistent with those of anode electrode. As a result, the SEI films on the electrodes surface formed by PTM can not only effectively alleviate the decomposition of carbonate-based electrolyte and $LiPF_6$ and avoid the attack of electrolyte on the electrodes, but also greatly decrease the interface resistance between electrolyte and electrodes, which are the fundamental reasons why the cells with PTM performed well over wide temperature ranges in the previous experiment. Furthermore, with the introduction of PTM additive, the stable and well-distributed SEI films can block the transfer of transition metal ions to anode. Based on the above results and analysis, the schematic diagram was presented in Fig. 7b, which clearly summarized the role of PTM as electrolyte additive.

4. Conclusion

In this paper, we demonstrated for the first time that the PTM as the electrolyte additive can not only enhance the stability of the electrolyte, but also greatly optimize the cycle performance of $LiNi_{0.6}Co_{0.2}Mn_{0.2}O_2$/graphite in the wide ranges of operating temperature. According to the results of the SEM, TEM, XRD, XPS and calculation simulation, we attribute the outstanding electrochemical performance to the formation of functional SEI films with the addition of PTM, which can not only effectively suppress the decomposition of carbonate-based electrolyte and $LiPF_6$ and protect electrodes from the electrolyte attack, but also generate the sulfur-based lithium salts to promote lithium conduction between the electrodes and electrolyte. Although many of the above characterizations are only tested with cells cycled at 25 °C, we believe that the above conclusions are universally applicable to explain the reason for the excellent performance of cells cycled at −20 °C and 45 °C. It can be expected that the application of electrolytes containing PTM in NCM-based LIBs has a bright future.

CRediT authorship contribution statement

Jingxiong Gao: Validation, Investigation, Data curation, Writing - original draft, Writing - review & editing, Visualization. **Songyi Han:** Conceptualization, Methodology, Validation, Investigation, Data curation, Writing - review & editing. **Haiming Hua:** Formal analysis, Software. **Jie Wu:** Validation, Formal analysis. **Jing Zeng:** Writing - review & editing. **Yuanyu Sun:** Validation, Formal analysis. **Weiping Tang:** Resources, Conceptualization, Methodology, Supervision. **Shuling Liu:** Resources, Writing - review & editing, Supervision. **Jinbao Zhao:** Writing - review & editing, Visualization, Supervision, Project administration.

Declaration of competing interest

The authors declare that they have no known competing financial interests or personal relationships that could have appeared to influence the work reported in this paper.

Acknowledgments

This work was financially supported by National Key Research and Development Program of China 2017YFB0102000, Scientific Research Planning Program of Key laboratory of Shaanxi Province of China (18JS015), Graduate Innovation Fund of Shaanxi University of Science and Technology.

Appendix A. Supplementary data

Supplementary data related to this article can be found online at https://doi.org/10.1016/j.jpowsour.2020.229416.

References

[1] Y. Ji, Y.C. Zhang, C.Y. Wang, Li-ion cell operation at low temperatures, J. Electrochem. Soc. 160 (2013) A636–A649.
[2] T.F. Yi, Y.M. Li, S.Y. Yang, Y.R. Zhu, Y. Xie, Improved cycling stability and fast charge-discharge performance of cobalt-free lithium-rich oxides by magnesium-doping, ACS Appl. Mater. Interfaces 8 (2016) 32349–32359.
[3] C.J. Chae, H.J. Noh, J.K. Lee, B. Scrosati, Y.K. Sun, A high-energy Li-ion battery using a silicon-based anode and a nano-structured layered composite cathode, Adv. Funct. Mater. 24 (2014) 3036–3042.
[4] T.L. Kulova, A.M. Skundin, High-voltage materials for positive electrodes of lithium ion batteries (review), Russ. J. Electrochem. 52 (2016) 501–524.
[5] C.C. Su, M. He, P.C. Redfern, L.A. Curtiss, I.A. Shkrob, Z. Zhang, Oxidatively stable fluorinated sulfone electrolytes for high voltage high energy lithium-ion batteries, Energy Environ. Sci. 10 (2017) 900–904.
[6] C.Y. Wang, G.S. Zhang, S.H. Ge, Terrence Xu, Y. Ji, X.G. Yang, Y.J. Leng, Lithium-ion battery structure that self-heats at low temperatures, Nature 528 (2016) 515–518.
[7] C. Xu, F. Jeschull, W.R. Brant, D. Brandell, K. Edström, T. Gustafsson, The role of LiTDI additive in $LiNi_{1/3}Mn_{1/3}Co_{1/3}O_2$/graphite lithium-ion batteries at elevated temperatures, J. Electrochem. Soc. 165 (2018) A40–A46.
[8] A. Barré, B. Deguilhem, S. Grolleau, M. Gérard, F. Suard, D. Riu, A review on lithium-ion battery ageing mechanisms and estimations for automotive applications, J. Power Sources 241 (2013) 680–689.
[9] T. Waldmann, M. Wilka, M. Kasper, M. Fleischhammer, M. Wohlfahrt-Mehrens, Temperature dependent ageing mechanisms in Lithium-ion batteries - a post-mortem study, J. Power Sources 262 (2014) 129–135.
[10] S.S. Zhang, K. Xu, T.R. Jow, Low temperature performance of graphite electrode in Li-ion cells, *Electrochim*, Acta 48 (2002) 241–246.
[11] S.S. Zhang, K. Xu, T.R. Jow, The low temperature performance of Li-ion batteries, J. Power Sources 115 (2003) 137–140.
[12] L.X. Liao, P.J. Zuo, Y.L. Ma, Y.X. An, G.P. Yin, Y.Z. Gao, Effects of fluoroethylene carbonate on low temperature performance of mesocarbon microbeads anode, Electrochim. Acta 74 (2012) 260–266.
[13] S.S. Zhang, K. Xu, T.R. Jow, Low-temperature performance of Li-ion cells with a $LiBF_4$ -based electrolyte, J. Solid State Electrochem. 7 (2003) 147–151.
[14] M.C. Smart, B.L. Lucht, S. Dalavi, F.C. Krause, B.V. Ratnakumar, The effect of additives upon the performance of MCMB/$LiNi_xCo_{1-x}O_2$ Li-ion cells containing methyl butyrate-based wide operating temperature range electrolytes, J. Electrochem. Soc. 159 (2012) A739–A751.

[15] B. Zhang, M. Metzger, S. Solchenbach, M. Payne, S. Meini, H.A. Gasteiger, A. Garsuch, B.L. Lucht, Role of 1,3-propane sultone and vinylene carbonate in solid electrolyte interface formation and gas generation, J. Phys. Chem. C 119 (2015) 11337–11348.
[16] B. Li, M. Xu, B. Li, Y. Liu, L. Yang, W. Li, S. Hu, Properties of solid electrolyte interphase formed by prop-1-ene-1,3-sultone on graphite anode of Li-ion batteries, Electrochim. Acta 105 (2013) 1–6.
[17] W. Yao, Z. Zhang, J. Gao, J. Li, J. Xu, Z. Wang, Y. Yang, Vinyl ethylene sulfite as a new additive in propylene carbonate-based electrolyte for lithium ion batteries, Energy Environ. Sci. 2 (2009) 1102–1108.
[18] J. Xia, N.N. Sinha, L.P. Chen, J.R. Dahn, A comparative study of a family of sulfate electrolyte additives, J. Electrochem. Soc. 161 (2014) A264–A274.
[19] D. Aurbach, K. Gamolsky, B. Markovsky, Y. Gofer, M. Schmidt, U. Heider, On the use of vinylene carbonate (VC) as an additive to electrolyte solutions for Li-ion batteries, Electrochim. Acta 47 (2003) 1423–1439.
[20] Gaussian 09, Revision E. 01, M.J. Frisch, G.W. Trucks, D.J. Fox, Gaussian, Inc., Wallingford CT, 2013.
[21] P.J. Stephens, F.J. Devlin, Ab initio calculation of vibrational absorption and circular dichroism spectra using density functional force fields, J. Phys. Chem. 98 (1994) 11623–11627.
[22] S. Grimme, J. Antony, A consistent and accurate ab initio parametrization of density functional dispersion correction (DFT-D) for the 94 elements H-Pu, J. Phys. Chem. 132 (2010), 154104.
[23] F. Weigend, R. Ahlrichs, Balanced basis sets of split valence, triple zeta valence and quadruple zeta valence quality for H to Rn: design and assessment of accuracy, Phys. Chem. Chem. Phys. 18 (2005) 3297–3305.
[24] V. Marenich, Cramer Aleksandr, J. Christopher Truhlar, G. Donald, Universal solvation model based on solute electron density and on a continuum model of the solvent defined by the bulk dielectric constant and atomic surface tensions, J. Phys. Chem. B 113 (2009) 6378–6396.
[25] T. Lu, F.W. Chen Multiwfn, A multifunctional wavefunction analyzer, J. Comput. Chem. 33 (2012) 580–592.
[26] T. Yang, W. Fan, C. Wang, Q. Lei, Z. Ma, L. Yu, X. Zuo, J. Nan, 2,3,4,5,6-Pentafluorophenyl methanesulfonate as a versatile electrolyte additive matches $LiNi_{0.5}Co_{0.2}Mn_{0.3}O_2$/graphite batteries working in a widetemperature range, ACS Appl. Mater. Interfaces 10 (2018) 31735–31744.
[27] B.W. Yang, H. Zhang, L. Yu, W.Z. Fan, Lithium difluorophosphate as an additive to improve the low temperature performance of $LiNi_{0.5}Co_{0.2}Mn_{0.3}O_2$/graphite cells, Electrochim. Acta 221 (2016) 107–114.
[28] Y.C. Lin, H. Zhang, Triallyl phosphite as an electrolyte additive to improve performance at elevated temperature of $LiNi_{0.6}Co_{0.2}Mn_{0.2}O_2$/graphite cells, J. Electroanal. Chem. 832 (2019) 408–416.
[29] S.K. Jung, H. Gwon, J. Hong, K.Y. Park, D.H. Seo, H. Kim, J. Hyun, W. Yang, K. Kang, Understanding the degradation mechanisms of $LiNi_{0.5}Co_{0.2}Mn_{0.3}O_2$ cathode material in lithium ion batteries, Adv. Energy Mater. 4 (2014), 1300787.
[30] J.G. Han, K. Kim, Y. Lee, N.S. Choi, Scavenging materials to stabilize $LiPF_6$-containing carbonate-based electrolytes for Li-ion batteries, Adv. Mater. 31 (2018), 1804822.
[31] J. Xia, J.E. Harlow, R. Petibon, J.C. Burns, L.P. Chen, J.R. Dahn, Comparative study on methylene methyl disulfonate (MMDS) and 1,3-propane sultone (PS) as electrolyte additives for Li-ion batteries, J. Electrochem. Soc. 161 (2014) A547. –A553.
[32] E.G. Leggesse, J.-C. Jiang, Theoretical study of the reductive decomposition of 1,3-propane sultone: SEI forming additive in lithium-ion batteries, RSC Adv. 2 (2012) 5439–5446.
[33] J. Chen, H. Zhang, M. Wang, J. Liu, C. Li, P. Zhang, Improving the electrochemical performance of high voltage spinel cathode at elevated temperature by a novel electrolyte additive, J. Power Sources 303 (2016) 41–48.
[34] B. Li, Y.Q. Wang, H.B. Lin, Performance improvement of phenyl acetate as propylene carbonate-based electrolyte additive for lithium ion battery by fluorine-substituting, J. Power Sources 267 (2014) 182–187.